Computation of Compressible, Laminar Boundary Layers on Swept, Tapered Wings

Harry P. Horton*
University of London,
London E1 4NS, England, United Kingdom
and
Hans-Werner Stock†
Dornier Luftfahrt GmbH, 82230 Wessling, Germany

Nomenclature

a = speed of sound
C = normalized density–viscosity product, $\rho\mu/(\rho\mu)_e$
C_p = pressure coefficient, $2(p - p_\infty)/\rho_\infty U_\infty^2$
c = chord length
c_{f_x} = local skin friction coefficient for circumferential flow, $2(\mu\partial u/\partial z)_w/\rho_e u_e^2$
f = transformed circumferential component of vector potential, $\psi_1(\theta, r, z)/(2\xi r/r_0)^{1/2}$
G = transformed radial component of vector potential (alternative), $(v_e/q_e)g$
g = transformed radial component of vector potential, $u_e\psi_2(\theta, r, z)/r(2\xi r/r_0)^{1/2}\tilde{v}_e$
H = total enthalpy
M_∞ = Mach number of undisturbed stream, U_∞/a_∞
p = static pressure
q_e = resultant external velocity, $\sqrt{u_e^2 + v_e^2}$
r = radial distance along generator, measured from cone apex, O
r_0 = radius of sphere centered at O, intersecting leading edge of streamwise section
S = enthalpy parameter, $H/H_e - 1$
T = static temperature
U_∞ = velocity of undisturbed stream
$(u, \tilde{v}, w)$ = velocity components in (θ, r, z) directions
v = spanwise velocity, $-\tilde{v}$
x = arc distance around surface, $r_0\theta$
y = spanwise distance, $r_0 - r$
z = distance normal to surface
γ = ratio of principal specific heat capacities of gas
Δ = transformed boundary-layer thickness
δ_x^* = displacement thickness of circumferential flow, $\int_0^z (1 - \rho u/\rho_e u_e)\,dz$
η = similarity variable used in present work, $u_e \int_0^z \rho\,dz/\sqrt{2\xi r/r_0}$
η_{K-C} = similarity variable used by Kaups and Cebeci, $\sqrt{v_e/\rho_e\mu_e r_0}\int_0^z \rho\,dz$
θ = polar angle in developed plane, measured from stagnation line
λ_1, λ_2 = sweep angles of leading and trailing edges
μ = coefficient of viscosity of gas
ξ = transformed circumferential coordinate, $\int_0^\theta \rho_e\mu_e u_e r_0\,d\theta$
ρ = mass density of gas
σ = Prandtl number of gas
ψ_1, ψ_2 = circumferential and radial components of vector potential

Subscripts
e = boundary-layer edge
s = stagnation line
w = wall
∞ = freestream

Superscript
$'$ = differentiation with respect to η

Received Feb. 15, 1995; revision received June 6, 1995; accepted for publication June 6, 1995.

*Senior Lecturer, Department of Aeronautical Engineering, Queen Mary and Westfield College. Member AIAA.
†Chief, Boundary Layer Aerodynamics Department, Postfach 1103, LREV 32, Gebäude 318.

Introduction

CURRENT interest in laminar flow technology has led to a demand for very accurate computer codes to generate velocity and temperature profiles in the laminar boundary layer on a swept wing. These profiles are required as input data for boundary-layer stability calculations, for which purpose smooth second derivatives with respect to z are necessary. For the greatest generality a fully three-dimensional boundary-layer method would be used, but for practical purposes the conical flow approximation of Kaups and Cebeci[1] provides a useful quasi-two-dimensional approach to analyzing the boundary layer on a swept, tapered wing of high AR, at a section where the isobars are essentially straight.

The Kaups–Cebeci computer code,[2] which has been widely distributed with the Sally stability code,[3] uses the Keller box method[4] to solve the boundary-layer equations after applying the transformation described in Ref. 1. Two types of difficulty arise in running the Kaups–Cebeci code, however. Firstly, Δ at the front stagnation line can vary by several orders of magnitude from case-to-case, so that initial values for the z-grid parameters have to be found by trial-and-error; Δ also varies strongly with streamwise distance. This is because the particular boundary-layer transformation used by Kaups and Cebeci is inappropriate. Secondly, and more seriously, severe oscillations in the second derivatives frequently occur close to the wall. This phenomenon may be attributed to the fact that the two-point centered-difference scheme, used for streamwise derivatives in the Keller box method, is only neutrally stable. Irregularities introduced into the computation either by poor choice of initial z grid or by lack of smoothness of the input pressure distribution are not well damped and cause the wiggles mentioned earlier. Both of these difficulties will be addressed here.

Boundary-Layer Equations

Following Kaups and Cebeci,[1] a section of a straight-tapered wing is treated as part of a conical wing with its apparent apex at O, as shown in Fig. 1. The cone section is defined by the line-of-flight wing section whose leading edge intersects r_0 centered at O, and curvilinear, orthogonal coordinates (θ, r, and z) are adopted, with r and θ lying in the surface. The case of an infinite swept wing (ISW) corresponds to $r_0 \to \infty$. The boundary-layer equations, given by Mager[5] for general curvilinear, orthogonal coordinates, then become

$$\frac{1}{r}\frac{\partial}{\partial\theta}(\rho u) + \frac{1}{r}\frac{\partial}{\partial r}(\rho r\tilde{v}) + \frac{\partial}{\partial z}(\rho w) = 0 \tag{1a}$$

$$\rho\left(\frac{u}{r}\frac{\partial u}{\partial\theta} + \tilde{v}\frac{\partial u}{\partial r} + w\frac{\partial u}{\partial z} + \frac{u\tilde{v}}{r}\right) = -\frac{1}{r}\frac{\partial p}{\partial\theta} + \frac{\partial}{\partial z}\left(\mu\frac{\partial u}{\partial z}\right) \tag{1b}$$

$$\rho\left(\frac{u}{r}\frac{\partial\tilde{v}}{\partial\theta} + \tilde{v}\frac{\partial\tilde{v}}{\partial r} + w\frac{\partial\tilde{v}}{\partial z} - \frac{u^2}{r}\right) = -\frac{\partial p}{\partial r} + \frac{\partial}{\partial z}\left(\mu\frac{\partial\tilde{v}}{\partial z}\right) \tag{1c}$$

$$0 = \frac{\partial p}{\partial z} \tag{1d}$$

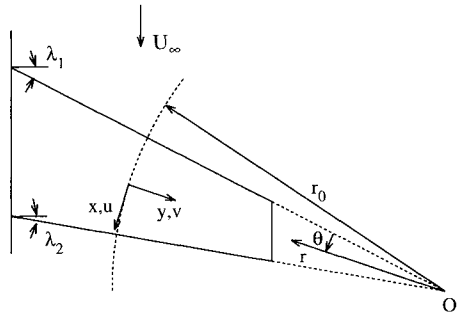

Fig. 1 Coordinate system for conical swept wing.

$$\rho\left(\frac{u}{r}\frac{\partial H}{\partial \theta} + \bar{v}\frac{\partial H}{\partial r} + w\frac{\partial H}{\partial z}\right) = \frac{\partial}{\partial z}\left\{\frac{\mu}{\sigma}\frac{\partial H}{\partial z} - \frac{1-\sigma}{\sigma}\mu\frac{\partial}{\partial z}\left[\frac{1}{2}(u^2 + \bar{v}^2)\right]\right\} \tag{1e}$$

The relevant boundary conditions are

$$\text{at} \quad z = 0, \quad u = \bar{v} = 0, \quad w = w_w$$
$$\text{and} \quad \frac{\partial H}{\partial z} = \left(\frac{\partial H}{\partial z}\right)_w \quad \text{or} \quad H = H_w \tag{1f}$$
$$\text{as} \quad z \to \infty, \quad u \to u_e, \quad v \to v_e, \quad H \to H_e$$

Following Kaups and Cebeci, it is now assumed that the radial pressure gradient $\partial p/\partial r$ is negligible, and $\partial u_e/\partial r$ and $\partial v_e/\partial r$ are similarly neglected. Continuity is satisfied by writing[6]

$$\rho u = \frac{\partial \psi_1}{\partial z}, \qquad \rho r \bar{v} = \frac{\partial \psi_2}{\partial z}, \qquad \rho w = -\frac{1}{r}\left(\frac{\partial \psi_1}{\partial \theta} + \frac{\partial \psi_2}{\partial r}\right) \tag{2}$$

Equations (2) differ somewhat from the comparable relations used by Kaups and Cebeci.

Boundary-Layer Transformation

Kaups and Cebeci use $\eta_{K\text{-}C}$, which superficially resembles the generalized Blasius variable. However, this does not correctly fulfill the main objective of using transformations in boundary-layer computations, which is to scale out the boundary-layer growth, so that roughly the same η grid can be used throughout; and consequently, to eliminate the leading-edge singularity so that the transformed equations reduce naturally to ordinary differential equations (ODEs) of universal form at the boundary-layer origin. It is also to be noted that the length scale in the denominator of the square-root in the definition of $\eta_{K\text{-}C}$ is a constant, in place of the streamwise distance used in the Blasius variable, and so the scaling does not conform with the expected parabolic growth of the boundary layer. Additionally, this transformation fails when $v_e = 0$, and therefore, cannot be used for wings with forward-swept trailing edges, neither does it give a proper limit to the ISW equations when $r_0 \to \infty$.

Here, η is introduced in order to remedy these deficiencies, and for convenience ξ is also used. Transformed dependent variables f, g, and S are introduced which, when the weak dependency of these variables on r is neglected in accordance with the conical flow approximation, results in a generalization of the well-known Levy[7] equations.

Some further minor changes in variables are convenient. Since all derivatives with respect to r have now been neglected, we may set $r = r_0$ and $x \equiv r_0\theta$ so that x is the distance from the stagnation line around the curve defined by the intersection of the conical wing with r_0, centered at O. For an ISW, x becomes the usual surface distance from stagnation, measured around a section normal to the leading edge. Also, following conventional notation for an ISW, put $y \equiv r_0 - r$ and $v \equiv -\bar{v}$. ξ and η now become the standard Levy variables, i.e.,

$$\xi = \int_0^x \rho_e \mu_e u_e \, dx, \qquad \eta = \frac{u_e}{(2\xi)^{1/2}}\int_0^z \rho \, dz \tag{3}$$

and the transformed boundary-layer equations take the final form

$$(Cf'')' + (f + 1.5Dg)f'' + \tilde{\beta}_x[(1 + S - f'^2) + E_{yx}(1 + S - g'^2)] + Df'(f' - g') = 2\xi\left(f'\frac{\partial f'}{\partial \xi} - f''\frac{\partial f}{\partial \xi}\right) \tag{4a}$$

$$(Cg'')' + (f + 1.5Dg)g'' + \beta_y^* f'(f' - g') = 2\xi\left(f'\frac{\partial g'}{\partial \xi} - g''\frac{\partial f}{\partial \xi}\right) \tag{4b}$$

$$(CS')' + \sigma(f + 1.5Dg)S' - 2(1 - \sigma) \times [C(E_x f'f'' + E_y g'g'')]' = 2\sigma\xi\left(f'\frac{\partial S}{\partial \xi} - S'\frac{\partial f}{\partial \xi}\right) \tag{4c}$$

where

$$\tilde{\beta}_x = (1 + m_{e_x})(\beta_x^* + D), \qquad \beta_x^* = 2\frac{d\,u_e/dx}{d\,\xi/dx}$$
$$\beta_y^* = 2\frac{d\,v_e}{d\,\xi}, \qquad D = -\frac{2}{r_0}\frac{v_e}{u_e}\Big/\frac{d\,\xi}{dx}$$
$$m_{e_x} = \left[\frac{(\gamma - 1)}{2}\right]\left(\frac{u_e}{a_e}\right)^2, \qquad m_{e_y} = \left[\frac{(\gamma - 1)}{2}\right]\left(\frac{v_e}{a_e}\right)^2 \tag{5}$$
$$m_e = m_{e_x} + m_{e_y}, \qquad E_x = \frac{m_{e_x}}{1 + m_e}$$
$$E_y = \frac{m_{e_y}}{1 + m_e}, \qquad E_{yx} = \frac{m_{e_y}}{1 + m_{e_x}}$$

The velocity, temperature, and density ratios are given by

$$u/u_e = f', \qquad v/v_e = g'$$
$$T/T_e = \rho_e/\rho = (1 + m_e)(1 + S) - (m_{e_x}f'^2 + m_{e_y}g'^2) \tag{6}$$

and the boundary conditions are

$$\text{at} \quad \eta = 0, \quad f = f_w, \quad f' = g = g' = 0$$
$$\text{and either} \quad S = S_w \quad \text{or} \quad S' = S'_w \tag{7}$$
$$\text{as} \quad \eta \to \infty \quad f' \to 1, \quad g' \to 1, \quad S \to 0$$

The previous system has the proper limiting behavior when $r_0 \to \infty$, when it reduces to an obvious generalization of the Levy equations for the ISW.

The parameter D is related to the divergence effect of taper and is zero for an ISW. β_y^* is simply related to this parameter by $\beta_y^* = (u_e/v_e)^2 D$, but is defined separately to avoid difficulties when $v_e = 0$.

The right-hand sides of Eq. (4) vanish at the boundary-layer origin, leaving a set of ODEs closely related to the equations at the origin of an ISW boundary layer, and do not

need the type of special treatment required in the Kaups–Cebeci formulation. Depending on whether the boundary layer originates at a stagnation line or a sharp leading edge, we have at $x = 0$ either, respectively,

$$\tilde{\beta}_{x_s} = 1 + D_s, \quad \beta^*_{y_s} = 0, \quad D_s = -\left[\frac{v_e}{r_0}\Big/\left(\frac{du_e}{dx}\right)\right]_s \tag{8a}$$

or

$$\tilde{\beta}_{x_s} = \beta^*_{y_s} = D_s = 0 \tag{8b}$$

The new transformation eliminates all of the difficulties associated with the Kaups–Cebeci transformation, with one exception. There is still a weak singularity at a point where v_e vanishes, when by definition g becomes infinite. If necessary, this singularity can be easily removed by redefining the spanwise variable as $G = (v_e/q_e)g$, where $q_e = (u_e^2 + v_e^2)^{1/2}$, so that $G' = \nu/q_e$. Substitution of this expression into Eqs. (4) results in the modified equations given in Ref. 8.

Numerical Method and Results

A Fortran code, QICTP1, has been written to solve the boundary-layer equations in the form just described. The geometric treatment of the wing is similar to that of Kaups and Cebeci, as is the method of calculation of external velocity components from an input pressure distribution. The numerical method used to solve Eqs. (4) (described in more detail in Ref. 8) is of the differential–difference type, in which ξ derivatives are approximated by three-point backward differences, resulting in a system of coupled ODEs with independent variable η to be solved at successive ξ stations, marching downstream. The two momentum equations and the energy equation are solved in sequence in an iterative loop as if uncoupled, the x-momentum equation being quasilinearized. Invariant imbedding is used to recast each of the three ODEs as an initial-value problem, the resulting stiff nonlinear equations being solved using a fourth-order accurate, implicit, stiffly stable Gear[9] method. The use of fully implicit ξ discretization eliminates the instability problem of the Keller box method, mentioned in the Introduction.

A second version of the code, QICTP2, incorporates the modifications outlined at the end of the previous section.

Comparisons are presented in Ref. 8 between results of the QICTP1 code and the Kaups–Cebeci code, which show excellent agreement for both velocity profiles and integral quantities; an example is given in Fig. 2. However, as Fig. 3 shows,

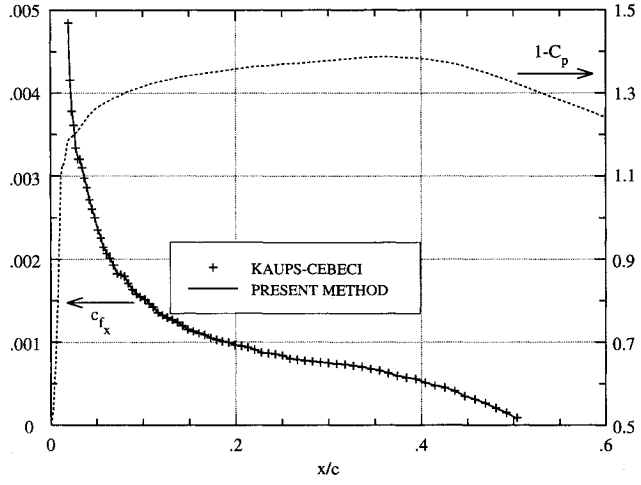

Fig. 2 Variation of c_{f_x} with x/c for boundary layer on upper surface of laminar flow section, $M_\infty = 0.1$, $\lambda_1 = 45$ deg, $\lambda_2 = 15$ deg, zero suction (case 1 of Ref. 8). Dashed curve shows pressure distribution.

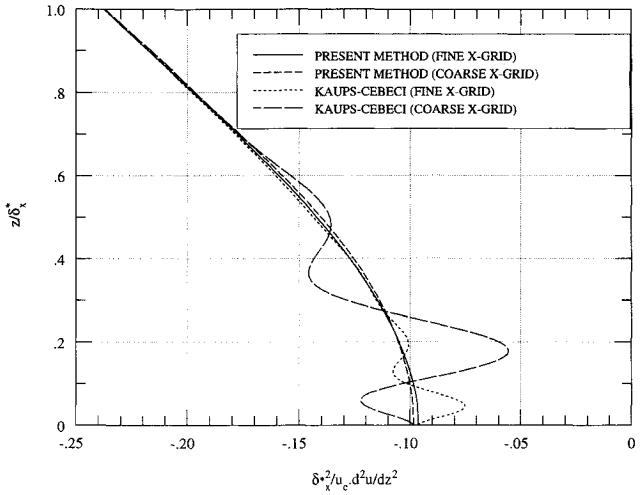

Fig. 3 Profiles of second derivative of circumferential velocity at $x/c = 0.1063$; same flow conditions as for Fig. 2. Coarse and fine grids have 45 and 90 x intervals, respectively.

the Kaups–Cebeci code (specifically, in the version distributed with Sally[3]) outputs second-derivative profiles exhibiting severe oscillations near the surface, which are absent from the QICTP1 results. Although in this case the amplitude of the oscillation is reduced when a finer x grid is used, the occurrence of the oscillations is unpredictable and may be provoked at the start of the computation by an unsuitable choice of grid normal to the surface.

Conclusions

The new transformation described previously has significant advantages over that used by Kaups and Cebeci for the computation of laminar boundary layers on swept, tapered wings. Because the boundary-layer growth is correctly incorporated into the new scalings, starting computations at the stagnation line is more straightforward, there are no significant streamwise variations of transformed boundary-layer thickness, and streamwise derivatives are minimized. Most importantly, computations using the new transformation, employing three-point backward streamwise differencing, are free of the spurious oscillations in second-derivative profiles that frequently occur in solutions of the Kaups–Cebeci equations using the Keller box method.

References

[1]Kaups, K., and Cebeci, T., "Compressible Laminar Boundary Layers with Suction on Swept and Tapered Wings," *Journal of Aircraft*, Vol. 14, No. 7, 1977, pp. 661–667.

[2]Kaups, K., and Cebeci, T., "Compressible Laminar Boundary Layers with Suction on Swept and Tapered Wings," Douglas Aircraft Corp., Rept. MDC J7337, Sept. 1976.

[3]Srokowski, A. J., and Orszog, S. A., "A FORTRAN Program to Compute and Integrate Disturbance Amplification Rates on Swept and Tapered Laminar Flow Control Wings with Suction," Computer Software Management and Information Center, Univ. of Georgia, Athens, GA, 1979.

[4]Keller, H. B., "A New Difference Scheme for Parabolic Problems," *Proceedings of the 2nd Symposium on the Numerical Solution of Partial Differential Equations*, edited by B. Hubbard, SYNSPADE 1970, Academic, New York, 1971, pp. 327–350.

[5]Mager, A., "Three-Dimensional Laminar Boundary Layers," *Theory of Laminar Flows*, edited by F. K. Moore, Sec. C, Princeton Univ. Press, Princeton, NJ, 1964, p. 290.

[6]Moore, F. K., "Three-Dimensional Compressible Laminar Boundary Layer Flow," NACA TN 2279, March 1951.

[7]Levy, S., "Effect of Large Temperature Changes (Including Viscous Heating) Upon Laminar Boundary Layers with Variable Free-Stream Velocity," *Journal of the Aeronautical Sciences*, Vol. 21, July 1954, pp. 459–474.

[8]Horton, H. P., "Computation of Compressible Laminar Boundary Layers on Swept, Tapered Wings," Queen Mary and Westfield College, Univ. of London, Faculty of Engineering Paper EP-1101, London, June 1995.

[9]Gear, C. W., "The Automatic Integration of Stiff Ordinary Differential Equations," *Information Processing, 68*, edited by A. J. H. Morel, North-Holland, Amsterdam, 1969, pp. 187–193.

Numerical Study of Alternate Forms of Dynamic-Stall-Vortex Suppression

M. C. Towne* and T. A. Buter†
U.S. Air Force Institute of Technology, Wright–Patterson Air Force Base, Ohio 45433

Nomenclature

C_l, C_d, C_m = lift, drag, and moment coefficients
C_μ = blowing coefficient, $\dot{m}_j V_j / q_\infty c$
c = chord
M = Mach number
$\dot{m}_j$ = mass flow rate of jet, $\rho_j s V_j \sin\phi$
q_∞ = dynamic pressure, $\frac{1}{2}\rho_\infty U_\infty^2$
Re_c = chord Reynolds number, $U_\infty c/\nu_\infty$
s = slot width
t^+ = nondimensional time, tU_∞/c
U_∞ = freestream velocity
V_j = velocity of jet
x, y = coordinates of moving reference frame attached to airfoil
α = angle of attack
α_b = onset angle of attack (blowing or suction)
ν = dynamic viscosity
ξ, η = transformed coordinates
ρ = density
ϕ = jet blowing angle, 10 deg
Ω^+ = nondimensional pitch rate, $\omega c/U_\infty$

Introduction

ATTEMPTS have been made by numerous researchers to harness the large aerodynamic forces temporarily generated on a streamlined body rapidly pitched beyond its steady stall angle of attack. Dynamically pitched airfoils exhibit maximum lift coefficients two or three times the static maximum lift.[1] Uncontrolled, the ensuing unsteady motion results in dynamic stall. The dynamic stall phenomenon arises in several applications: wind turbine blades, helicopter rotor blades, jet engine compressor blades, and rapidly pitched airfoils. The current study compares and contrasts two approaches to dynamic stall suppression: 1) suction and 2) nearly tangential blowing, applied in the vicinity of the leading edge of a NACA 0015 airfoil.

Dynamic stall suppression via leading-edge suction and leading-edge tangential blowing focuses on the removal of low momentum fluid that accumulates along the airfoil upper surface as it is pitched upward. Specifically, as the airfoil is pitched up, the adverse pressure gradient along the upper surface promotes the forward propagation of reverse-flowing fluid into the leading-edge region. The thickening of this low momentum fluid region near the leading edge ultimately forces an upward displacement and "kinking" of the feeding shear layer. The kinking of this shear layer marks the initial formation of the dynamic stall vortex. Suction experiments by Karim and Acharya[2] demonstrated that the key to dynamic-stall-vortex-formation suppression is to remove fluid from underneath the leading-edge-originating shear layer at the same rate as the reverse-flowing-fluid-pooling accumulation rate. Results by Towne[3] verify their findings numerically and demonstrate that tangential blowing applied upstream and/or in this pooling region is also effective in eliminating the low momentum region, and hence, in delaying dynamic stall vortex (DSV) formation.

The flow regime of interest is one of low speed and low Reynolds number. A compressible Navier–Stokes code developed by Visbal to numerically investigate dynamic stall[4,5] is used. The nominal flow and pitch-rate conditions are $M_\infty = 0.2$, $Re_c = 2.4 \times 10^4$, and $\Omega_0^+ = 0.2$.

Numerical Methodology

The strong conservation law form of the two-dimensional compressible Navier–Stokes equations are cast in an inertial frame of reference using a general time-dependent coordinate transformation to account for the motion of the body. Closure of the system is provided by the perfect-gas law, Sutherland's viscosity formula, and the assumption of a constant Prandtl number.

Freestream conditions are imposed at the inflow boundary. At the surface, no-slip adiabatic conditions are used. At the outflow far-field boundary, velocity and density are extrapolated and pressure is set to the freestream pressure. For the current simulation, an O-grid structure is employed. This necessitated the specification of periodic boundary conditions at the O-grid cut by overlapping five grid points in the ξ direction. To simulate the nearly tangential jet the velocity at the slot location was specified with a given magnitude and orientation. The pressure boundary condition was not modified at the slot. The flowfield for time-periodic flow at zero angle of attack is used as the initial condition.

To avoid the expense of regridding at every time level, a grid that is fixed relative to the airfoil was used. An extensive grid study was conducted on mesh sizes ranging from 203 to 505 points in the ξ direction (circumferential) and 101 to 301 points in the η direction.[3] Each grid was applied to a physical domain that extends nominally 30 chord lengths away from the airfoil. The current results were obtained on a 361×201 grid that had minimum ξ and η spacings of 0.000082 and $0.00005c$, respectively. No fewer than 21 grid points were used to define the slot aperture. The governing equations were numerically solved using the alternating direction implicit approximate-factorization algorithm of Beam and Warming.[6] Fourth-order explicit and second-order implicit spectral damping was used to damp high-frequency numerical oscillations and enhance stability behavior.

Results and Discussion

In a previous numerical study by Towne,[3] nearly tangential blowing was applied at a series of locations along the airfoil upper surface to assess the effect of slot position on DSV suppression. Based upon this work and the suction experiment of Karim and Acharya,[2] the comparison between suction and blowing was conducted for a single slot position of width $0.00717c$ at $x/c = 0.05$. The selection of this position assured that the slot was located upstream of the point at which the DSV was seen to form in the natural (no-control) case. Previous work by Towne and Buter[7] showed that blowing applied aft of the natural DSV vortex formation point, while useful for retarding the forward propagation of reverse flow from the trailing edge, did not suppress the formation of the dynamic stall vortex.

Received April 12, 1995; revision received May 16, 1995; accepted for publication May 16, 1995.

*Assistant Professor. Member AIAA.
†Assistant Professor. Senior Member AIAA.